ELSEVIER

Ceramics International 26 (2000) 887–895

CERAMICS INTERNATIONAL

Factors affecting the microstructure of a fine ceramic foam

H.X. Peng [a], Z. Fan [a], J.R.G. Evans [b,*]

[a] *Department of Materials Engineering, Brunel University, Uxbridge, Middlesex UB8 3PH, UK*
[b] *Department of Materials, Queen Mary and Westfield College, University of London, Mile End Road, London E1 4NS, UK*

Received 1 September 1999; received in revised form 7 September 1999; accepted 13 September 1999

Abstract

Sintered cellular ceramics with varying degrees of reticulation were prepared using coarse and fine alumina powders and a 70/30 mixture thereof. The ceramic foams had fine cell size (about 150 μm diameter) in each case. The method of preparation involved the free expansion of suspensions of these powders at 20 vol.% in a polyurethane foaming system. In order to modify the microstructure, the expansion was opposed using a die, and this reduced the void fraction and window size. In addition, directional rising was achieved by expanding the foam in a long cylindrical vessel and this modified the cell shape of the final foam. These foams have potential use in a range of applications including catalysis, but the main aim of the present work was to prepare preforms for metal matrix composites.

Keywords: B. Microstructure; Ceramic foams

1. Introduction

Open cell or reticulated ceramic foams are used mainly in applications where fluid transport in the microstructure is needed [1]. The cell size and degree of reticulation depend on the method of manufacture. Recent reviews of ceramic foams and their fabrication include those by Saggio-Woyansky et al. [2], Sepulveda [3] and Rice [4]. The other potential application of open-cell foams is to produce two phase, three-dimensionally inter-connected composites by melt infiltration [5]. This provides an effective way to control the distribution of the reinforcement in composite materials and of particular interest are metal matrix composites (MMCs).

Generally, the fabrication method selected determines the range of porosity, the pore morphology and pore size distribution. It is often difficult to control the degree of reticulation. For example, the sol–gel method produces a foam with a cell size in the nanometer range [3] while a porous ceramic prepared by the infiltration and replication of a polymer foam offers pores in the millimetre range but normally produces hollow struts [6,7].

The foaming method described here produces fine open-cell porous ceramics. Previous work has indicated that conventional and commercially available polyurethane systems can be used to produce ceramic foams [8–10]. Such systems are widely available and are ideal if microstructural control of the final foam during the processing step is required. In particular, from the point of view of producing MMCs, a composite with controlled distribution of reinforcement is believed to yield better overall performance [11].

This paper, based on the method established in our previous work [10,12], shows the capability for microstructural control of ceramic foams by varying the starting materials and processing parameters.

2. Experimental details

2.1. Starting materials

A two-component, polyurethane (PU) foam system (grade ISOFOAM RM6216W) was supplied by Baxenden Chemicals (Accrington, Lancashire, UK). The details were described elsewhere [12].

The ceramic powders selected for this study were Alcan MA130 and RA45E which are predominantly alpha-alumina (Al_2O_3) with D_{50} of 4 and 0.48 μm, respectively. They were donated by Alcan Chemicals, Gerrards Cross, UK. Fig. 1 shows the morphology of the particles and

* Corresponding author. Tel.: +44-027-975-5154. fax: +44-027-975-5150.

0272-8842/00/$20.00
PII: S0272-8842(00)00032-8

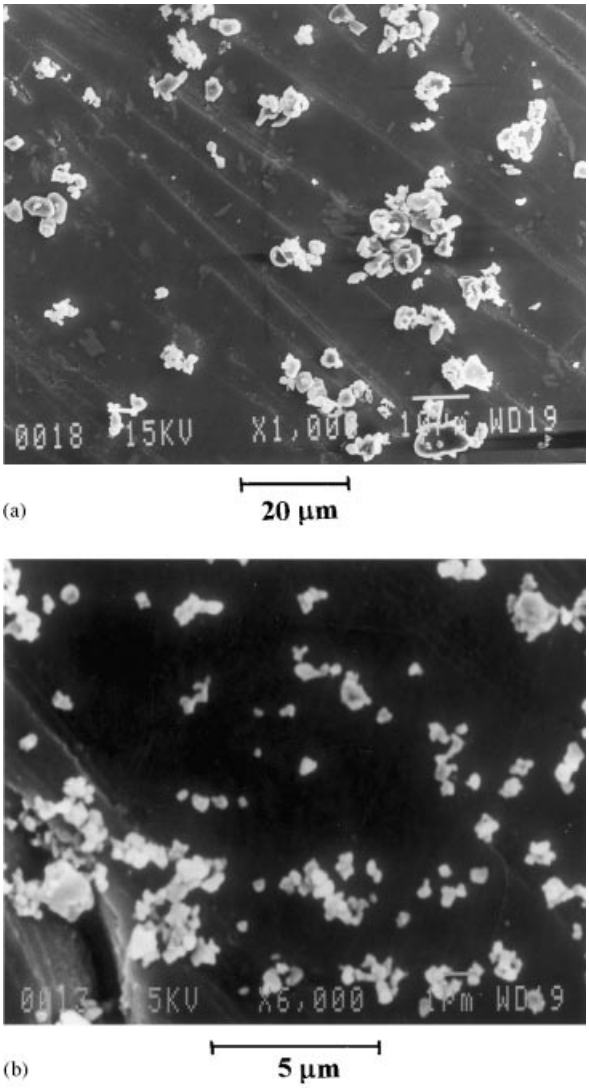

Fig. 1. Scanning electron micrograph of (a) coarse MA130 alumina and (b) fine RA45E alumina.

the particle size distributions (PSD) are shown in Fig. 2. A mixture with a coarse to fine ratio of 70:30 of these powders was prepared by mixing on a rolling mill for 24 h at a speed of 60 rpm in alcohol with alumina media. The mixture was then dried to a final temperature of 280°C.

To assess the flow properties of the suspensions used for foam preparation, mixtures of the powders with the polyol component were prepared. The three alumina powders were introduced into this component by stirring at 2400 rpm, and the suspensions were tested using a Model 2ARES/3A Rheometer (Rheometrics Scientific Ltd, Surrey Business Park, Surrey, UK) fitted with parallel plate geometry with a gap of 1 mm suitable for testing low viscosity liquids and operated at 25°C. Although viscosity cannot be deduced from this measurement, a comparative value of an apparent viscosity can be calculated using the rim shear rate.

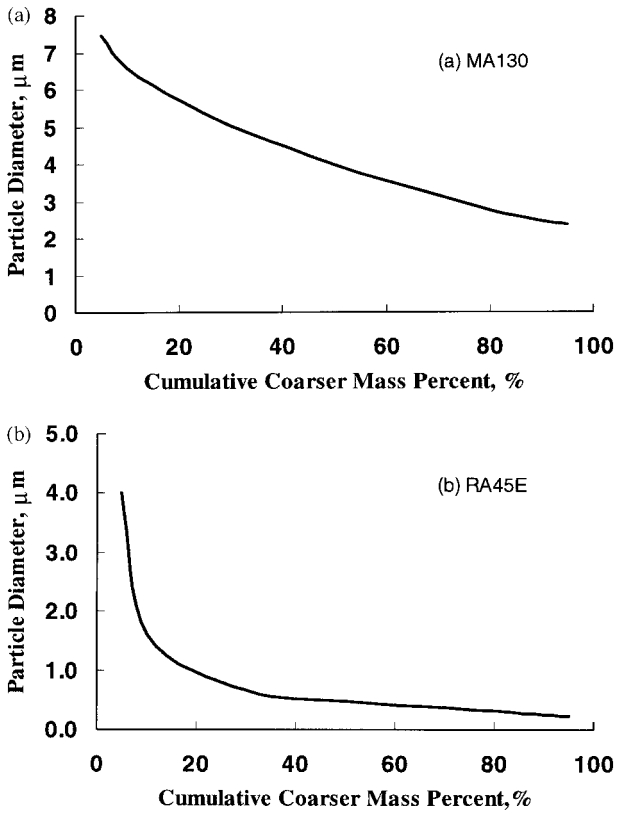

Fig. 2. Particle size distributions of (a) MA130 alumina and (b) RA45E alumina.

2.2. Foam preparation

The processing sequence is summarized in Fig. 3 and the details are given in another paper [12]. Essentially the powder is stirred into each of the component liquids. These are then stirred together for less than 1 min. and poured into the mould. All the suspensions prepared for foaming contained 20 vol.% powder mixed into both components of the system. Three parameters were changed as shown in Table 1. In the first instance, the foam rising process was opposed by carrying out the expansion in a die fitted with a free floating piston loaded with deadweights from which the opposing pressure could be deduced. This has the effect of restricting the volume of the foam and of modifying microstructural features. In the second case, the foam rising direction was limited by pouring the 'cream' into a long (360 mm) cylindrical vessel with an inner diameter of 65 mm. In the third case, a ceramic powder blend with a different particle size distribution was used for the purpose of investigating the effect of powder size on the microstructure of the final foam.

The polymer–ceramic foam was cut into cubes of side 40 mm and pyrolysed in flowing air (4 l/h) at 5°C/h to 450°C with a 2 h hold before furnace cooling. Sintering was carried out in air with a heating rate of 2°C/min to 1650°C with a 2 h hold before furnace cooling.

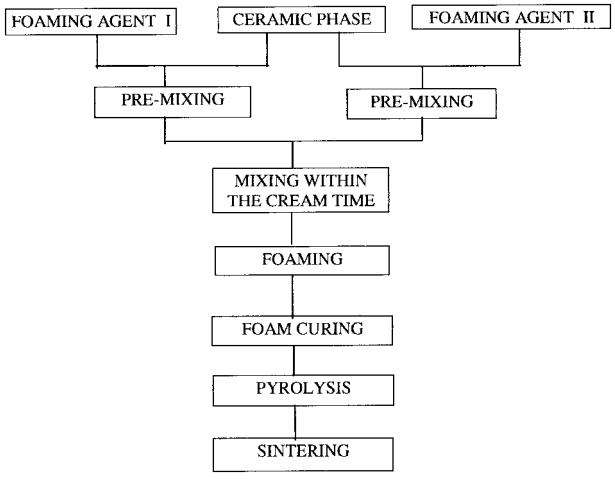

Fig. 3. Flow-chart describing the stages involved in the preparation of ceramic foams.

2.3. Microstructual characterization and compression testing

The microstructure of the foams was observed by using a Jeol JX840 scanning electron microscope and the compressive strength of the sintered foam was measured using a Model 4206 Instron testing machine (Instron Ltd, Buckinghamshire, UK) fitted with flat steel platens closing with a cross head speed of 0.5 mm/min.

Table 1
Processing details for the ceramic foams

Designation	Powder size (D_{50}) (μm)	Expansion limit (%)	Pressure (kPa)
MA130	4	100	0
MA130–87%[a]	4	87	7.63
MA130–80%[a]	4	80	11.2
RA45E	0.48	100	0
70/30 Mixture	–	Directional	0

[a] Restricted expansion.

3. Results and discussion

3.1. Effect of applied pressure on the foam microstructure

Taking the volume of the foam which is allowed to rise freely as V_0, and the volume of a foam which expands under imposed pressure as V', the ratio of V' to V_0 can be treated as the expansion limit, K:

$$K = V/V_0 \quad (1)$$

The pressures used to oppose expansion in the cavity and the corresponding expansion limits are given in Table 1. The volumes decreased as the pressure increased within a pressure range which presents no serious laboratory hazard (Table 1).

The density of alumina is 3987 kg m^{-3} and the density of the polyurethane was taken as 1150 kg m^{-3} [10] giving the density of the ceramic-polymer system as 1717 kg m^{-3}. The measured apparent densities of the foams are given in Table 2 from which the pore volume fraction can be found. For the MA130 foams with $K = 1$, 0.87 and 0.8, respectively, the specific volumes were 8×10^{-3}, 6.8×10^{-3} and 6.33×10^{-3} m^3 kg^{-1}, respectively. These measured specific volumes for the restricted expansion foams correspond to the ratios 0.85 and 0.79 for $K =$ 0.87 and 0.8, respectively.

The microstructure of the MA130 foamed sample which was restricted to 80% expansion ($K = 0.8$) before pyrolysis and sintering is shown in Fig. 4. From this it can be seen that with the restricted degree of rising, the foam appears to be completely closed cell with abundant powder present in the windows. The freely foamed suspensions have some obviously transparent windows which consist of a thin polymer film which contains no ceramic powder [10]. More details of the struts are shown in Fig. 4b, in which most of the ceramic powder resides. Although the ceramic powder has been thoroughly mixed with the polymer phase, the cell wall is very smooth and unpunctured by particles. It is possible to see what

Table 2
Microstructure parameters of the sintered ceramic foams

Samples	MA130 100% rising	MA130 87% rising	MA130 80% rising	RA45E 100% rising	70/30 Mixture[a]
Cell size D (μm)	150±16[a]	149±19[a]	151±18[a]	152	–
Window size d (μm)	72	57	49	74	–
As-foamed density (kg m^{-3})	125	147	158	121	115
As-foamed porosity (%)	92.7	91.4	90.7	93.0	93.3
Sintered foam relative density	0.055	0.069	0.077	0.061	0.063
Porosity (%)	94.5	93.1	92.3	93.9	93.7
d/D	0.48	0.38	0.33	0.49	–
Predicted porosity from Eq. (3) (%)	95	89	86	96	–

[a] 95% confidence limits.

appears to be a particle-depleted layer at the surface reminiscent of the particle migration noted in shear flow [13]. Whether this occurs adjacent to a free surface in elongational flow as it does in shear flow has yet to be explored. The effect could be due to flocculation of the suspension which would also cause phase separation.

The foams were then pyrolysed and sintered and fracture faces were prepared for scanning electron microscopy. This allowed window and cell size to be estimated from cells which presented an equator in the fracture surface and from windows by taking the major axis of oblique windows as the true diameter. The microstructural parameters summarized in Table 2 include the average cell size and window size. The window size increases with the degree of expansion and hence with the void volume fraction as shown by a simple quantitative model based on ordered packing [12]. In each foam, the average cell size was about 150 μm. The uniformity of cell diameter, seen in Fig. 5, is related to the foaming process in which the final stage of ripening is associated

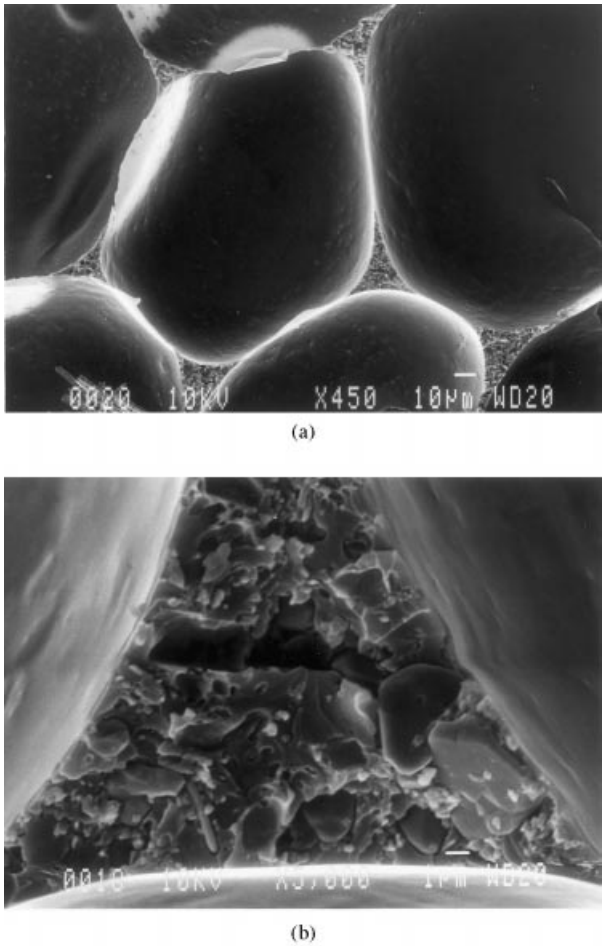

Fig. 4. Microstructure of polymer/ceramic foam before pyrolysis (80% MA130) showing (a) cell wall and fractured struts, and (b) the fracture surface of a strut.

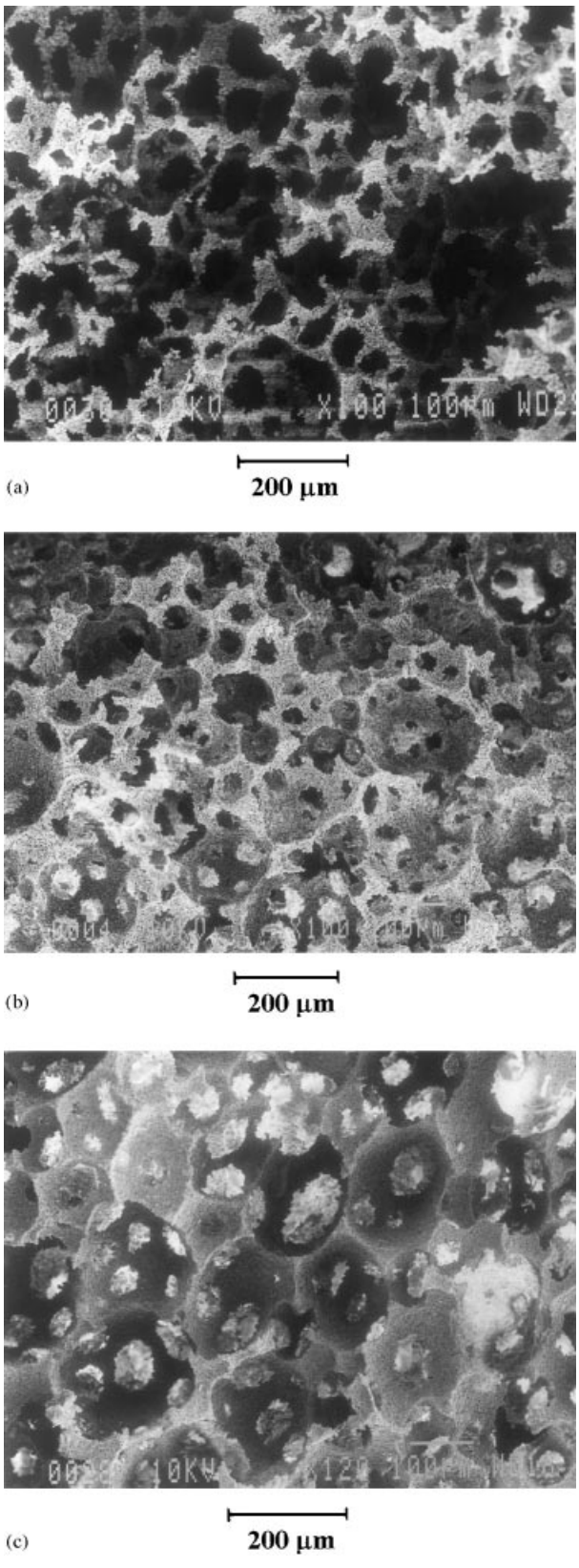

Fig. 5. Comparison of the microstructure of sintered MA130 alumina foams produced with different degrees of expansion: (a) 100%, unrestricted; (b) 87%; (c) 80%.

with the loss of smaller bubbles and a reduced growth rate of large bubbles giving a more uniform distribution of cell diameters [14].

The cell size (the bubble size) is mainly controlled by the following factors:

1. the gas generation capability which for a given system should be a constant;
2. the nucleation and growth of bubbles, involving inter-alia, the diffusion of gas from small to larger bubbles;
3. the number of bubbles finally existing in the system.

The pressure developed during restrained foaming is not expected to affect the nucleation of bubbles hence it should not reduce the initial number of bubbles in the system. Arefmanesh and co-workers [15], studying bubble growth in a polymeric foaming process, derived an expression for the bubble radius as a function of time. The growth rate $\bar{R}$, for a Newtonian fluid under isothermal conditions can be expressed by

$$\bar{R} = \frac{1}{4\eta}[(P_g - P_f)R - 2\sigma] \quad (2)$$

where η is the viscosity, σ the surface tension, P_g the gas pressure inside the bubble, and $P_f$the applied pressure at the outer boundary of the liquid. Thus, increasing the applied pressure (P_f), should cause the growth rate to decrease and lead to a smaller cell size.

The expected behaviour is therefore, reduction of cell diameter and thickening of the struts with the overall number of cells unchanged. In fact, the cell diameter, within the experimental error, remained unchanged while the window size decreased. However, the degree of expansion was restricted to 80%, and for a fixed number of cells, the corresponding cell diameter should decrease by only 7% which lies well within the error associated with measurement as indicated by the 95% confidence limits given in Table 2.

The microstructures of the sintered MA130 foams with different degrees of expansion are shown in Fig. 5. The window size in this series of foams clearly decreases with decreasing degree of expansion. The free-rising foam possesses the highest degree of reticulation. The degree of reticulation can be expressed in terms of the ratio of window size to cell size k, for cellular ceramics and can be related to the pore volume fraction, V_p, for a pore co-ordination number of 12 [12] by:

$$V_p = \frac{\pi}{\sqrt{2}}\left[\frac{3}{1-k^2} - \frac{5}{3}\left(\frac{1}{\sqrt{1-k^2}}\right)^3 - 1\right] \quad (3)$$

In Table 2 the predicted and measured values of final pore volume fraction, V_p, are compared. This shows that the use of an opposing pressure has caused the windows to close slightly more than predicted by the model for the restricted MA130 foams. For the remaining foams, the model correlates well with measured V_p.

From Fig. 5, it is also clear that the thickness of the struts in different foams also varies. The higher the degree of expansion, the thinner is the strut, and the strut strength is expected to be lower. This is reflected in the compressive strength results which are discussed below.

3.2. Effects of PSD on the foam structure

The mean particle diameter of the powder exerts a significant influence on the viscosity of the polyurethane ceramic suspension [16,17], and hence, on the flow behaviour of the suspension during the foaming process. The introduction of ceramic powder results in an increase in viscosity of the components of the foam which can be estimated from expressions which consider the ceramic volume fraction in the low volume fraction regime. An example is the expression suggested by Batchelor [18]

$$\eta = \eta_s(1 + 2.5\phi + 6.2\phi^2) \quad (4)$$

where η is the viscosity of the suspension, η_s is the viscosity of the suspending medium and ϕ is the volume fraction of particles. According to this, the addition of 20% powder should provide a 75% increase in viscosity but the situation is complicated by the fact that, while the unfilled resin components are nearly Newtonian, the filled systems are shear-thinning. Fig. 6 shows an "apparent viscosity" deduced from a parallel plate geometry using the rim shear rate. When comparing the elongational and shear viscosities, the shear viscosity should be evaluated at a strain rate $\sqrt{3}\dot{\varepsilon}$ where $\dot{\varepsilon}$ is the elongational strain rate [19]. Nevertheless the elongational strain rates associated with foam expansion are in a range two or three orders below the shear rates explored and so the difference in viscosities is much greater than that

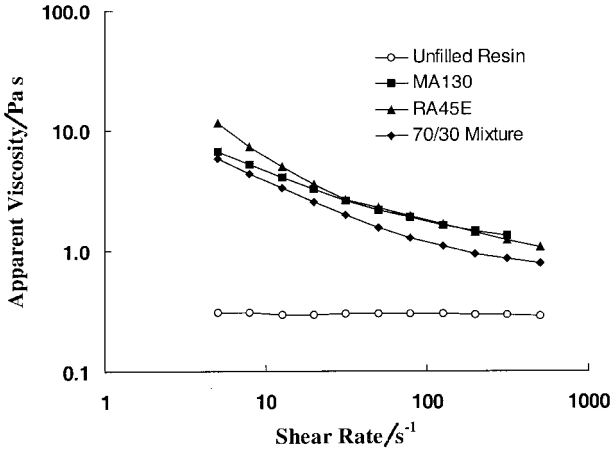

Fig. 6. Apparent viscosity — shear rate curves of unfilled and filled resins (parallel plate geometry was used and the rim shear rate is quoted).

predicted by Eq. (4) because of the shear thinning behaviour. The main deduction from Fig. 6 is that these suspensions are poorly stabilized flocculating systems. This is evident from the high degree of shear thinning presented by relatively dilute (20 vol.%) suspensions [20]. It supports the idea that phase separation may occur and powder retreats in the struts of the foam to leave a polymer-rich surface layer as observed above. These results also show that though the effect of powder blending is to give a lower viscosity than either parent powder, the reduction in viscosity is only about 40%.

Table 3 gives a summary of the relative densities and volumetric shrinkages at each stage in the process. For each foam, a substantial shrinkage occurs as the polymer is removed and particles, which are initially packed at a relative density of 20%, approach and make contact. Thus the shrinkage on pyrolysis establishes the prefired relative density at which the particle assemblies enter the sintering furnace. It is interesting to note that the fine alumina undergoes a very high shrinkage at this stage to pack efficiently before firing and giving a prefired density of 57% which is comparable to that which would emerge from compaction or injection moulding for a comparable powder. The coarse platey powders are relatively immobile at this stage and no packing advantage from the blending of coarse and fine powder emerges from inspection of the prefired relative densities.

The calculations of prefired relative density are based on the assumption that cells remain part of the macrostructure at this stage and similarly the calculation of final sintered relative density is based upon the assumption that cell walls have too large a radius of curvature to take part in sintering compared with interparticle pores. This assumption turns out to be invalid for the fine powder as evidenced by the calculated relative density which is found to be greater than unity. This indicates that cells of ~150 μm diameter do contribute to sintering and confirms the microstructural observation that the fine alumina approaches full density after sintering.

Figs. 7a and b show scanning electron micrographs of the sintered foams made from fine (RA45E) powder while the foam made from coarse (MA130) powder under identical processing conditions is shown in Fig. 7c. Both of these are free rising foams. Clearly, the struts in the fine powder foam are more dense. Although it is well known that the PSD affects the packing density of powder

Table 3
Volumetric shrinkage and relative density of the struts calculated on the assumption that foam cells do not participate in sintering

Foam	Initial relative density[a]	Volumetric shrinkage on pyrolysis	Prefired relative density	Volumetric shrinkage on sintering	Sintered relative density[b]
MA130–100	0.2	0.46	0.37	0.37	0.58
MA130–87	0.2	0.50	0.40	0.31	0.56
RA45E	0.2	0.65	0.57	0.52	1.18[c]
70/30	0.2	0.48	0.39	0.43	0.67

[a] Of ceramic powder based on the ceramic–polymer binary system.
[b] Refers to the ceramic struts excluding the cells.
[c] A calculated value > 1 indicates some cells participated in sintering.

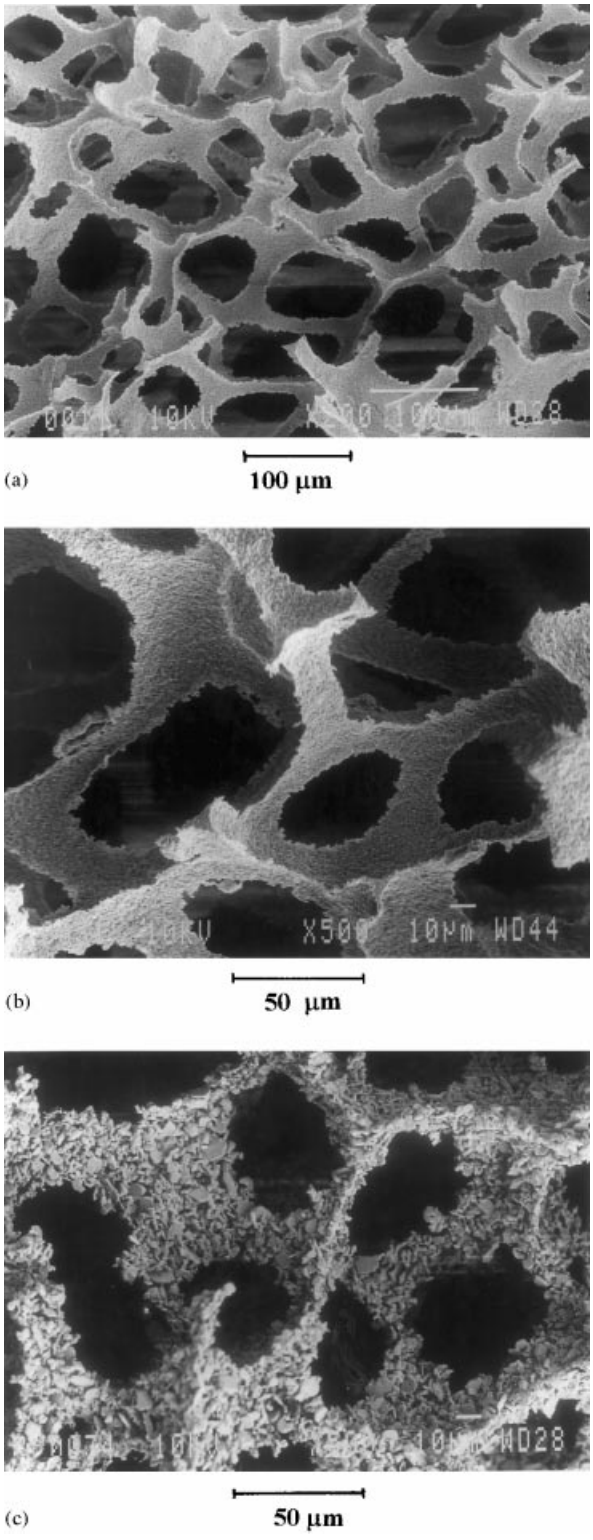

Fig. 7. Microstructure of sintered foams made with fine RA45E alumina: (a) low magnification; (b) showing structure of the struts; (c) foam made with coarse MA130 powder.

compacts [17], this effect was not observed in the struts of the sintered ceramic foams as shown by the prefired relative densities in Table 3. The packing efficiency was no better than that for the unblended MA130 powder. The main reason for this is that the prefired relative density is attained as the organic constituents are displaced by pyrolysis and it relies on particle movement to progress from 0.2 to 0.4 fractional relative density. The large platey particles are evidently less mobile than the fine alumina particles which progress from 0.2 to 0.57 at this stage. During sintering, the fine powder progresses to a high relative density and the calculated value in Table 3 shows that some of the small cells have contributed to sintering. The coarse powder attains about 60% relative density and the powder blend, influenced mainly by the fine constituent, reaches about 70%.

From the MMC point of view, a loosely packed strut gives the chance for the melt to infiltrate it which reduces the possibility of interfacial separation under the influence of differential thermal contraction. On the other hand, dense struts, which are 3-dimensionally continuous, can be used to produce a composite with an interpenetrating network which is a very attractive kind of material and expected to possess high performance [21].

3.3. Directional foaming

The microstructure of the directionally foamed product made with a 70/30 coarse/fine powder blend is shown in Fig. 8. Along the foam rising direction, both cell shape and window shape are elongated as indicated in Fig. 8a. Fig. 8b shows the microstructure perpendicular to the foam expansion direction in which the cells maintain their circular section. This technique provides a simple way to introduce microstructural anisotropy into the foam.

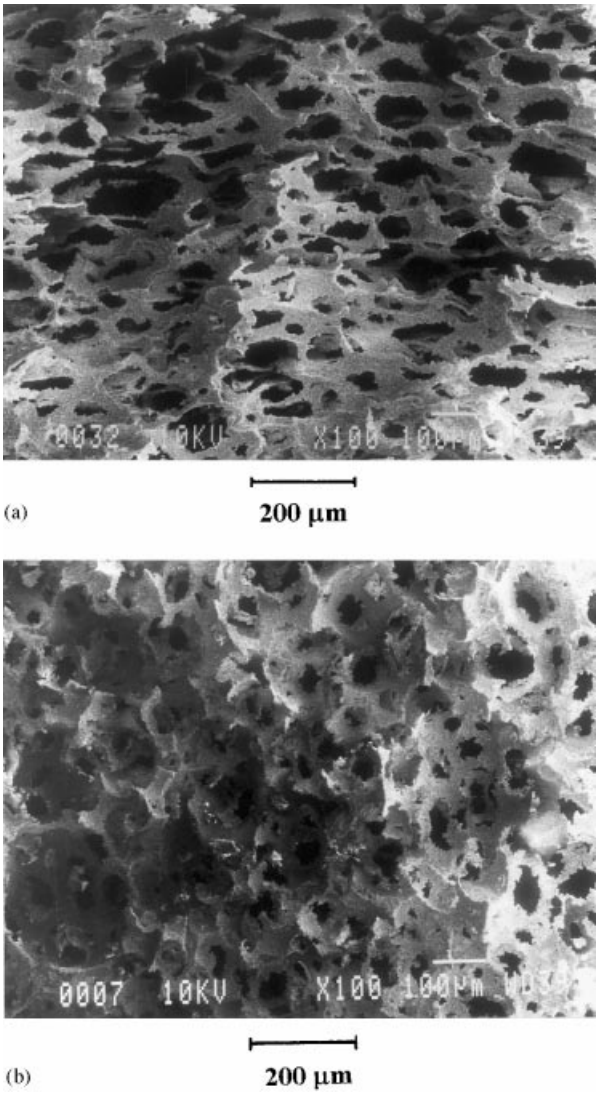

Fig. 8. Microstructure of sintered directionally constrained foam in the (a) longitudinal and (b) transverse direction.

3.4. Compressive behaviour of ceramic foams

Fig. 9 is a typical stress-strain curve for the ceramic foams under compression testing. In the initial stage, after the cross-head had contacted the sample, the load increased linearly. When the applied load exceeded a certain value, the sample started crushing and the load maintained a constant value. The nominal stress deduced from this load can be defined as the crushing strength [22]. The curve exhibits a horizontal plateau and, during this stage, the sample became progressively damaged (layer by layer) from either the top or the bottom due to the breakage of struts [22].

Fig. 10 shows the compressive strength of the foams as deduced from the horizontal plateau for different degrees of foam expansion. The compressive strength of the foam increases with the decrease of the degree of expansion and hence with increased solids volume fraction as expected. The foams with lower degrees of expansion possess smaller window size and thicker struts. The strength of the strut has a direct effect on that of the ceramic foam.

Studies of brittle cellular materials have demonstrated a relationship between the mechanical behaviour and relative density ρ/ρ_s. Generic expressions have the form

$$\text{Foam property/solid property} = C(\rho/\rho_s)^n \quad (5)$$

where C is a geometric constant characteristic of the unit cell shape, ρ_s is the theoretical density and n depends on the deformation mode of the struts [22].

Models developed to explain this behaviour rely on the assumption that the mechanics of a single unit cell can be used to describe the global deformation behaviour of the foam. Such models conclude that the most important factor affecting the mechanical behaviour is the relative density, but they also identify some influence of the cell size on the properties. The following expression

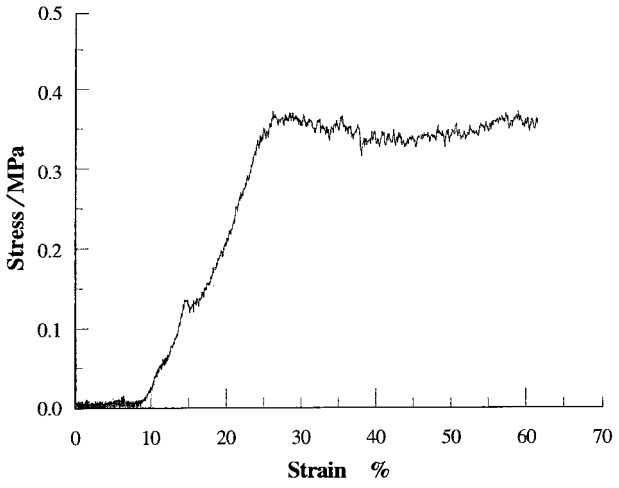

Fig. 9. Typical compressive stress–strain curve of the ceramic.

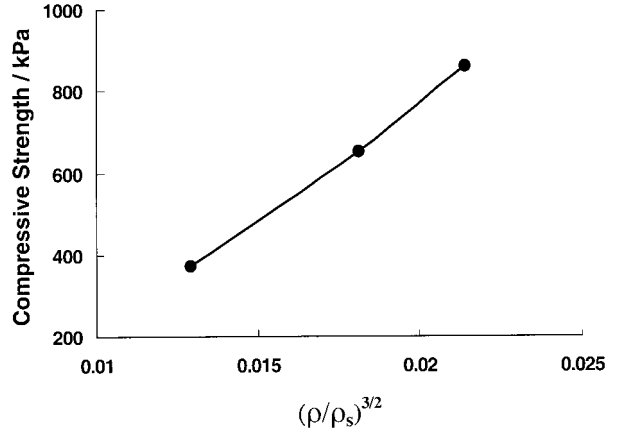

Fig. 10. Compressive strength as a function of relative density.

was developed to describe the dependence of compressive strength (σ_{fc}) of open cell ceramics on relative density [22]

$$\sigma_{fc}/\sigma_{fs} = C(\rho/\rho_s)^{3/2} \quad (6)$$

here, C is a constant that depends on the cellular geometry and has been found empirically to be approximately 0.2 for brittle open-cell foams, σ_{fs} is the fracture strength of the parent material, for a brittle solid, it is close to the fracture stress in simple tension.

The compressive strengths for the foams investigated in the present work increase with the total volume fraction of ceramic as predicted by Eq. (6). Taking the tensile strength of alumina as 260 MPa [23] and putting the data into Eq. (6), the strengths obtained are lower than predicted due mainly to the porous incompletely sintered struts. On the other hand, if the constant C is taken as 0.15, the predicted values meet the experimental data well.

From the melt infiltration point of view, for aluminium matrix composites, the strengths recorded here are high enough to withstand the melt infiltration pressure. Several studies of infiltration of preforms have been carried out [24-26]. Low speed infiltration is desirable and the limiting pressure is taken as the capillary pressure for a non-wetting fluid. On this basis, the lower strength limit for infiltration of such a porous foam is about 100 kPa, estimated by taking the window size of 40 μm. During squeeze casting, the melt is expected to infiltrate the cells first, and later to fill pores in the struts.

4. Conclusions

By employing a polyurethane foaming system, alumina foams with fine cell size (~150 μm diameter) have been prepared. The microstructures of these foams were controlled by varying the processing parameters. Without significantly changing the cell size, the window diameter was effectively modified by opposing the foam rise. With increasing degree of expansion, the window size and the void fraction increased. The cell aspect ratio can be varied by directional foaming using a narrow mould. The same preparation parameters can be used for different powders and the density of the struts can be influenced by changing the particle size distribution of the starting materials. The compressive strength of the foams increased with the decreasing degree of expansion suggesting that the strength of the struts increased. These foams have potential use in a range of applications including catalysis, but the fine reticulated foams prepared here provide an ideal microstructure for the preparation of metal matrix composites by melt infiltration to provide bi-continuous interpenetrating networks. In such applications, incomplete sintering of the struts may allow the liquid metal to penetrate the open pores of the ceramic skeleton.

Acknowledgement

The authors are grateful to EPSRC for funding this work under Grant No. GR/L80553.

References

[1] L.A. Strom, T.B. Sweeting, D.A. Norris, J.R. Morris, Novel applications of fully sintered reticulated ceramics, Mater. Res. Soc. Symp. Proc. 371 (1995) 321–326.
[2] J. Saggio-Woyansky, C.E. Scott, W.P. Minnear, Processing of porous ceramics, Am. Ceram. Soc. Bull. 71 (11) (1992) 1674–1682.
[3] P. Sepulveda, Gelcasting foams for porous ceramics, Am. Ceram. Soc. Bull. 76 (10) (1997) 61–65.
[4] R.W. Rice, The porosity dependence of physical properties of materials: a summary review, Key Eng. Mater. 115 (1996) 1–19.
[5] R. Brezny, D.J. Green, The effect of cell size on the mechanical behaviour of cellular materials, Acta Metall. Mater. 38 (12) (1990) 2517–2526.

[6] K. Schwartzwalder, A.V. Somers, Method of making porous ceramic articles, US Patent No. 3090094, 21 May 1963.
[7] F.F. Lange, K.T. Miller, Low density ceramics fabricated from reticulated polymer substrates, Adv. Ceram. Mater. 2 (4) (1987) 827–831.
[8] L.L. Wood, P. Messina, K.C. Frisch, Method of preparing porous ceramic structures by firing a polyurethane foam that is impregnated with inorganic materials, US Patent No. 3833386, 3 September 1974.
[9] W.P. Minnear, Processing of foamed ceramics, in: M.J. Cima (Ed.), Ceramic Transactions 26: Foaming Science and Technology for Ceramics, Am. Ceram. Soc., Westerville, OH, 1992, pp. 149–156.
[10] S.J. Powell, J.R.G. Evans, The structure of ceramic foams prepared from polyurethane–ceramic suspensions, Materials and Manufacturing Processes 10 (4) (1995) 757–771.
[11] Z. Fan, A microstructural approach to the effective transport properties of multiphase composites, Phil. Mag. A 73 (6) (1996) 1663–1684.
[12] H.X. Peng, Z. Fan, J.R.G. Evans, J.J.C. Busfield, Microstructure of ceramic foams, J. Eur. Ceram. Soc. 20 (7) (2000) 807–813.
[13] F. Gauthier, H.L. Goldsmith, S.G. Mason, Particle motion in non-Newtonian media, II. Poiseuille flow, Trans. Soc. Rheol. 15 (1971) 297–330.
[14] J.H. Saunders, R.H. Hansen, The mechanism of foam formation, in: K.C. Frisch, J.H. Saunders (Eds.), Plastic Foams, Part I, Marcel Dekker, New York, 1972, pp. 23–108.
[15] A. Arefmanesh, S.G. Advani, E.E. Michaelides, A numerical study of bubble growth during low pressure structural foam molding process, Polym. Eng. Sci. 30 (20) (1990) 1330–1338.
[16] Z. Fan, A.R. Boccaccini, A new approach to the effective viscosity of suspensions, J. Mater. Sci. 31 (1996) 2515–2521.
[17] Rheology of suspensions, in: H.A. Barnes, J.F. Hutton, K. Walters (Eds.), An Introduction to Rheology, Rheology Series, 3, Elsevier Science Publishers Amsterdam, 1989, pp. 115-140.
[18] G.K. Batachelor, The effect of Brownian motion on the bulk stree in a suspension of spherical particles, J. Fluid Mech. 83 (1997) 97–117.
[19] D.M. Jones, K. Walters, P.R. Williams, On the extensional viscosity of mobile polymer solutions, Rheol. Acta 26 (1987) 20–30.
[20] H.A. Barnes, Shear thickening in suspensions of non-aggregating solid particles dispersed in Newtonian liquid, J. Rheol. 33 (1989) 329–336.
[21] D.R. Clarke, Interpenetrating phase composites, J. Am. Ceram. Soc. 75 (4) (1992) 739–759.
[22] Gibson, L.J. Ashby, M.F. Cellular Solids: Structure and Properties, 2nd edition, Cambridge Solid State Science Series, Cambridge University Press, 1997, pp. 209–217.
[23] L.D. Hart, Alumina Chemicals: Science and Technology Handbook, The American Ceramic Society, 1990.
[24] D.K. Biswas, J.E. Gatica, S.N. Tewari, Dynamic analysis of unidirectional pressure infiltration of porous preforms by pure metals, Metall. Mater. Trans. 29A (1998) 377–385.
[25] K.P. Trumble, Spontaneous infiltration of non-cylindrical porosity: close-packed spheres, Acta Mater. 46 (7) (1998) 2363–2367.
[26] A. Mortensen, J.A. Cornie, On the infiltration of metal matrix composites, Metall. Trans. A 18A (1987) 1160–1163.